

A wavelet frame coefficient total variational model for image restoration

Wei Wang*, Xiang-Gen Xia*[†], and Shengli Zhang*

September 30, 2018

Abstract

In this paper, we propose a Rudin-Osher-Fatemi(ROF)-like model for image restoration which utilizes total variation (TV) regularization on the wavelet feature images. The model imposes more smoothing power on the cartoon image generated by the low-pass filter and less strength on the edges generated by the high-pass filters. Thus, the model can preserve more edges and details than the ROF model. Next, the existence of solution for the model was proved and a slightly modified split Bregman algorithm was used to solve it. At last, we present some experimental results to show its competitive advantage to the related methods both in quality and efficiency.

keywords. Image restoration, wavelet, total variation, variational method

1 Introduction

Image restoration including image denoising, deblurring, inpainting etc. is a procedure of improving the quality of a given image that is degraded in various ways during the process of acquisition and commutation; and enabling us to obtain crucial but imperceptible information existing in the image. Since many advanced applications in computer vision depend heavily on the input of high quality images, image restoration becomes an indispensable and preprocessing step of these applications. Therefore, image restoration is a basic but very important area in image processing and analysis. Image restoration can be modeled as a linear inverse problem:

$$f = Au + \eta$$

*College of Information Engineering, Shenzhen University, Shenzhen, China.
(aiyulunhui@sina.com, xxia@ee.udel.edu, zsl@szu.edu.cn)

[†]Department of Electrical and Computer Engineering, University of Delaware, Newark, DE 19716, USA.

This research is partially supported by the research grants from the Chinese NSF project (61372078), National Natural Science Foundation of China (No. 61701320), Guangdong NSF project (2014A030313549), Key project of Guangdong (2016KZDXM006) and the Shenzhen NSF project (JCYJ20160226192223251).

where f is the observed images, A is a linear operator representing the blur (usually a convolution) and η represents the additive noise whose type depends on its probability density function (PDF). The goal of image restoration is to find the unknown true image u from the observed image f . The problem is usually an ill-posed inverse problem and often solved by imposing a prior regularization assumption. Among all regularization-based methods for image restoration, variational based and wavelet frames based methods have attracted a lot of attention in the past.

The common assumption of the regularization based methods is that images can be sparsely approximated in some transformed domains. Such transforms can be gradient operator, wavelet frame transform, Fourier transform, Gabor transform etc. In order to utilize the sparsity, one solves (1) by finding a sparse solution in the corresponding transformed domain. Typically, the l_1 norm is used as a penalty of the sparsity. One of the famous variational approaches is the Rudin-Osher-Fatemi (ROF) model, which imposes the total variation (TV) regularization on the image u :

$$\inf_{u \in BV(\Omega)} \left\{ \lambda \int_{\Omega} |\nabla u| + \int_{\Omega} (u - f)^2 dx \right\}.$$

Here, Ω is the image domain, $BV(\Omega)$ is the bounded variational space, $\int_{\Omega} |\nabla u|$ and $\int_{\Omega} (u - f)^2 dx$ are the TV (regularization) term and fidelity (fitting) term, respectively. The ROF model performs well for removing noise while preserving edges. However, it tends to produce piecewise constant results (called staircase effect in the literature). After the ROF model was proposed, the TV regularization has been extended to many other image restoration applications (such as deblurring, inpainting, superresolution, etc.) [1][2][3][4][5][6][7] and has been modified in a variety of ways to improve its performance [8][9][10][11]. To solve the ROF model, many algorithms have been proposed [12][13][14][15][16][17][18] and the split Bregman method is the one of the most widely used [16].

Wavelet frames represent images as a summarization of smooth components (i.e. cartoon), and local features (i.e. singularities). In wavelet frame domain, smooth image components are the coefficient images obtained from low-pass filters, while local features are those obtained from high-pass filters. Thus, we can impose different strength of regularization on smooth components and local features separately when restoring images in the wavelet frame transform domains. There exist plenty of wavelet frame based image restoration models in the literature, such as, the synthesis based approach [19][20][21][22], the analysis based approach [23][24][25][26], and the balanced approach [27][28][29]. A typical analysis based model of l_1 norm regularization has a similar form with the ROF model:

$$\min_u \lambda \|Wu\|_1 + \frac{1}{2} \|Au - f\|_2^2,$$

where W represents the wavelet frame transform. Since the l_1 norm regularizations usually exist in the wavelet frame based models, the split Bregman algorithm is also a widely used method to solve them.

In this paper, we propose a ROF-like model for image restoration by combining the TV regularization and wavelet frame based models. Unlike the ROF model and the traditional wavelet frame based models, we impose the TV regularization on the coefficient images rather than the TV norm or the l_1 norm. In addition, the proposed model imposes more smoothing power on the cartoon coefficient generated by the low-pass filter and less strength on the edges and details coefficients generated by the high-pass filters. By this way, our model can preserve more edges and details than the ROF model which imposes the same smoothing power on all the spatial pixels. At last, the split Bregman algorithm is used to solve the model and some numerical simulations are presented to show the superiority of our method to the related models.

The rest of the paper is organized as follows. In Section 2.1, we describe the proposed model and prove the existence of its solution. In Section 2.2, we use the split Bregmann algorithm to solve the model. In Section 3, we present some experimental results to show the advantage of our model. In Section 4, we conclude this paper.

2 The wavelet coefficient total variational model

2.1 Proposed model

Before describing the model, we briefly introduce the discrete wavelet transform. Note that in the literature, there are two kinds of wavelet transforms: decimated and undecimated. Since every level coefficient (feature) images generated by the undecimated wavelet transforms have the same size of the original, which is more natural to our model, we adopt the undecimated version in this paper.

Define the two-dimensional discrete wavelet transform, or the analysis operator with L levels of decomposition as

$$Wu = \{W_{l,m,n}u : l = 0, 1, \dots, L-1; m, n = 0, 1, \dots, r\},$$

where

$$W_{l,m,n}u = (h_m^l)^T h_n^l \otimes (h_0^{l-1})^T h_0^{l-1} \otimes (h_0^{l-2})^T h_0^{l-2} \dots \otimes (h_0^1)^T h_0^1 \otimes u, \quad (1)$$

\otimes represents the matrix convolution and h_m^l is the row vector obtained by inserting zeros into the analysis filter h_m with factor 2^l .

The inverse (synthesis) wavelet transform is denoted as S . By the unitary extension principle (UEP) in [30], we have $S = W^*$, where W^* is the adjoint operator of W . Hence

$$W^*Wu = u \quad (2)$$

The wavelet transform decomposes the image into different feature images based on the different filters. The one generated by the low-pass filter is the cartoon and those by the high pass-filters are the edges and details (see figure 3). When an image is corrupted by noises, all its feature images are contaminated. In this paper, we propose a variational model for image restoration

which imposes TV regularization on the wavelet feature images. In addition, the proposed model imposes more smoothing power on the cartoon image generated by the low-pass filter and less strength on the edges and details generated by the high-pass filters. By this way, our model can preserve more edges and details than the ROF model which imposes the same smoothing power on all the spatial pixels.

The proposed model is described as following:

$$\arg \min_{u \in BV(\Omega)} E(u) = \left\| \nabla(\vec{\lambda} \cdot W u) \right\|_1 + \frac{1}{2} \|Au - f\|_2^2 \quad (3)$$

where W denotes the wavelet transform, $(\vec{\lambda} \cdot W u)_{l,m,n} = \lambda_{l,m,n} W_{l,m,n} u$ and ∇ is the gradient operator. In this paper, we set all the value of $\lambda_{l,m,n} = \lambda_1 > 0$ equally except for $\lambda_{L,0,0} = \lambda_0 > \lambda_1$.

If $W = 1$, we have that problem (11) is reduced to the TV model. If the frame is orthonormal, then $E(u)$ can be rewritten as

$$\sum_j \left\| \nabla(\lambda_j \cdot u_{\varphi_j}) \right\|_1 + \frac{1}{2} \left\| (Au)_{\varphi_j} - f_{\varphi_j} \right\|_2^2$$

and problem (3) is equivalent to the following problem:

$$\arg \min_{u_{\varphi_j} \in BV(\Omega)} E(u_{\varphi_j}) = \left\| \nabla(\lambda_j \cdot u_{\varphi_j}) \right\|_1 + \frac{1}{2} \left\| (Au)_{\varphi_j} - f_{\varphi_j} \right\|_2^2 \quad (4)$$

where $u_{\varphi_j} = \langle u, \varphi_j \rangle$ is the wavelet coefficient of frame basis φ_j . Clearly, problem (4) is the total variational model for every coefficient image u_{φ_j} . Thus, when the wavelet frame is orthonormal, the proposed model is equivalent to denoising the feature images first and then synthesizing the final clean image. In the literature, there are some papers [31][32][33][34][35][36][37][38][39][40] utilizing the similar ideas. However, our model is different from them. Since the redundant wavelet frames are not orthonormal, our model is not fully equivalent to (4) and can only be seen as a ROF-like model using a different regularization term. Moreover, most of the above papers tackle images in the transform domain and obtain the restored images by the inverse wavelet transform while our model is solved directly in the spatial domain.

In the following, we show the existence of the solution for problem (3).

Theorem 1. If the operators W , W^* and A are linear and bounded, $\|A \otimes 1\|_{L^2(\Omega)} \neq 0$, where \otimes is the convolution and Ω is the image domain, then problem (3) admits a solution in $BV(\Omega)$.

Proof. Let $\{u_n\}$ be a minimizing sequence of problem (3). Then there exists a constant $M > 0$ such that $E(u_n) \leq M$, i.e.

$$\left\| \nabla(\vec{\lambda} \cdot W u_n) \right\|_1 + \frac{1}{2} \|Au_n - f\|_2^2 \leq M \quad (5)$$

from which we get

$$\frac{1}{2} \|Au_n - f\|_2^2 \leq M \quad (6)$$

and

$$\|\nabla(\vec{\lambda} \cdot Wu_n)\|_1 \leq M \quad (7)$$

Let $\|W^*\|_1 \leq C$. Then from inequality (7), we obtain

$$\|W^*\nabla(\vec{\lambda} \cdot Wu_n)\|_1 \leq \|W^*\|_1 \|\nabla(\vec{\lambda} \cdot Wu_n)\|_1 \leq CM \quad (8)$$

Since the operators ∇, W can be seen as convolutions, they can interchange orders. Thus by inequality (8), we have

$$\lambda_1 \|\nabla u_n\| \leq \lambda_1 \|W^*W\nabla u_n\| = \|W^*\nabla(\lambda_1 Wu_n)\| \leq \|W^*\nabla(\vec{\lambda} \cdot Wu_n)\|_1 \leq CM \quad (9)$$

which implies that the total variation of $\{u_n\}$ is uniformly bounded.

From inequality (6) and $\|A \otimes 1\|_{L^2(\Omega)} \neq 0$, we can get that the sequence $\{u_n\}$ is bounded in $L^2(\Omega)$ which was proved in [41]. Hence u_n is bounded in $L^1(\Omega)$. Since the total variation of $\{u_n\}$ is also bounded, we get that u_n is bounded in $BV(\Omega)$. Therefore, there exists $u^* \in BV(\Omega)$ such that u_n converges to u^* weakly in $L^2(\Omega)$ and strongly in $L^1(\Omega)$. Since the operator W is linear bounded, we have Wu_n converges to Wu^* weakly in $L^2(\Omega)$ and strongly in $L^1(\Omega)$. Then a standard process can show that u^* is a minimizer of $E(u)$. \square

2.2 Algorithm

In this section, we utilize the split Bregman algorithm [16] to solve problem (3). Let $d = \nabla(Wu)$, $d^0 = b^0 = 0$, then problem (3) is equivalent to the following iterations:

for $j=0,1,2$,

$$u^{j+1} = \arg \min \frac{1}{2} \|Au - f\|_2^2 + \frac{\vec{\gamma}}{2} \|\nabla(Wu) - d^j + b^j\|_2^2 \quad (10)$$

$$d^{j+1} = \vec{\lambda}|d|_1 + \frac{\vec{\gamma}}{2} \|d - \nabla(Wu^{j+1}) - b^j\|_2^2 \quad (11)$$

$$b^{j+1} = b^j + (\nabla(Wu^{j+1}) - d^{j+1}) \quad (12)$$

Here, like λ , we set the value of $\gamma_{l,m,n} = \gamma_1 > 0$ equally except for $\gamma_{L,0,0} = \gamma_0 > \gamma_1$. The reason for the slight modification is that we want to smooth the feature images generated by the low-pass filter $h_0^T h_0$ to a higher degree.

By (1) and (2), the KKT condition for problem (10) is

$$\begin{aligned}
& A^*(Au - f) + W^* \nabla^* (\vec{\gamma} \cdot (\nabla(Wu) - d^j + b^j)) \\
&= A^*(Au - f) + \nabla^* \nabla (W^* (\vec{\gamma} \cdot Wu)) - \nabla^* W^* (\vec{\gamma} \cdot (d^j - b^j)) \\
&= A^*(Au - f) + \nabla^* \nabla \left(\sum_{l,m,n} \gamma_{l,m,n} W_{l,m,n}^* W_{l,m,n} u \right) - \nabla^* W^* (\vec{\gamma} \cdot (d^j - b^j)) \\
&= A^*(Au - f) + \gamma_1 \nabla^* \nabla (W^* Wu) \\
&\quad + (\gamma_0 - \gamma_1) \nabla^* \nabla (W_{L-1,0,0}^* W_{L-1,0,0} u) - \nabla^* W^* (\vec{\gamma} \cdot (d^j - b^j)) \\
&= A^*(Au - f) + \gamma_1 \nabla^* \nabla (u) \\
&\quad + (\gamma_0 - \gamma_1) \nabla^* \nabla (A_0 \otimes A_1 \dots A_{L-1} \otimes B_0 \otimes B_1 \dots B_{L-1}) \otimes u - \nabla^* W^* (\vec{\gamma} \cdot (d^j - b^j)) \\
&= 0
\end{aligned}$$

where $A_l = (h_0^l)^T h_0^l$, $B_l = (g_0^l)^T g_0^l$ and g_0^l is the row vector obtained by inserting zeros into the synthesis filter g_0 with factor 2^l . Therefore, the solution for problem (10) is

$$u^{j+1} = FFT^{-1} \left(\frac{FFT(\nabla^* W^* (\vec{\gamma} \cdot (d^j - b^j)) + A^* f)}{FFT(A^* A + \gamma_1 \nabla^* \nabla + (\gamma_0 - \gamma_1) \nabla^* \nabla (A_0 \dots A_{L-1} B_0 \dots B_{L-1}))} \right) \quad (13)$$

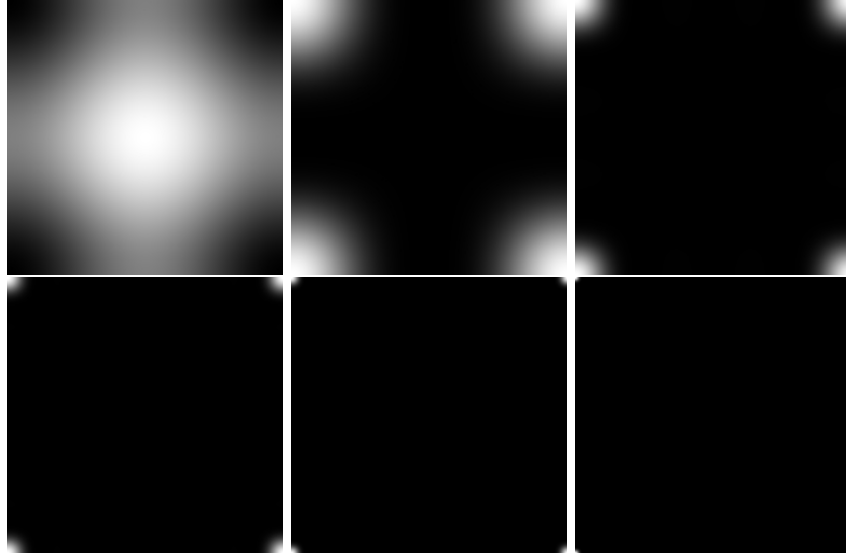


Figure 1: From left to right, from up to down are: FFTs of $\nabla^* \nabla$ and $A_0 \dots A_{L-1} B_0 \dots B_{L-1}$ with $L = 1, 2, 3, 4, 5$, respectively.

In Figure 1, we show the Fast Fourier transform (FFT) of $\nabla^* \nabla$ and $A_0 \dots A_{L-1} B_0 \dots B_{L-1}$ with different L , where $h_0 = g_0 = [0.25, 0.5, 0.25]$. From Figure 1, we can see that when $L > 2$, the FFT of $A_0 \dots A_{L-1} B_0 \dots B_{L-1}$ is almost zero. Also, we can observe that the effect of the term $A_0 \dots A_{L-1} B_0 \dots B_{L-1}$ is opposite to that of $\nabla^* \nabla$. Since the effect of $\nabla^* \nabla$ is smoothing the image, the

term $A_0 A_1 \dots A_{L-1} B_0 B_1 \dots B_{L-1}$ may slow down the convergence speed and cause artifacts in the denoised images. Thus in the numerical simulations, we neglect the term $\nabla^* \nabla (A_0 \dots A_{L-1} B_0 \dots B_{L-1})$ for computational efficiency. Equation (13) is thus changed into

$$u^{j+1} = \text{FFT}^{-1} \left(\frac{\text{FFT}(\nabla^* W^* (\vec{\gamma} \cdot (d^j - b^j)) + A^* f)}{\text{FFT}(A^* A + \gamma_1 \nabla^* \nabla)} \right) \quad (14)$$

Equation (14) can be seen as a analogy of the original split Bregman algorithm who solves u^{j+1} by

$$u^{j+1} = \text{FFT}^{-1} \left(\frac{\text{FFT}(\nabla^* (\gamma_1 \cdot (d^j - b^j)) + A^* f)}{\text{FFT}(A^* A + \gamma_1 \nabla^* \nabla)} \right)$$

By experiments, we find that using equation (14) can indeed get better results and make the algorithm converge faster than using equation (13).

The solution for problem (11) is

$$d^{j+1} = TH(\nabla(Wu^{j+1}) + b^j, \vec{\lambda}/\vec{\gamma}) \quad (15)$$

where $TH(x, T) = \text{sgn}(x) \max(|x| - T, 0)$.

At last, the algorithm is summarized in Algorithm 1 below:

Algorithm 1

Set the initial values $d^0 = b^0 = 0$, $k = 0$, the maximal iteration $M > 0$ and the tolerant error $tol \geq 0$.

while $j < M$ and $\frac{\|u^{j+1} - u^j\|}{\|u^k\|} > tol$ **do**

 Update u^{j+1} , d^{j+1} and b^{j+1} by equations (14), (15) and (12), respectively.

end while

return u^{j+1}

3 Experimental results

In this section, we conduct some numerical experiments on image denoising and image deblurring using Algorithm 1. In all of the numerical simulations, the piecewise linear B-spline wavelet frame is used for W and the level of decompositions is set as $L = 1$. The filter banks of the B-spline wavelet frame are

$$[h_0(-1), h_0(0), h_0(1)] = \frac{1}{4}[1, 2, 1]$$

$$[h_1(-1), h_1(0), h_1(1)] = \frac{\sqrt{2}}{4}[1, 0, -1]$$

$$[h_2(-1), h_2(0), h_2(1)] = \frac{1}{4}[-1, 2, -1]$$

and

$$\begin{aligned}[g_0(-1)g_0(0), g_0(1)] &= \frac{1}{4}[1, 2, 1] \\ [g_1(-1), g_1(0), g_1(1)] &= \frac{\sqrt{2}}{4}[-1, 0, 1] \\ [g_2(-1), g_2(0), g_2(1)] &= \frac{1}{4}[-1, 2, -1]\end{aligned}$$

In Section 3.1, we compare the experimental results of our model with the related methods (such as split Bregman algorithm (SB) [16], dual tree complex wavelet transform (DTCWT) [42], local contextual hidden markov model (LHMM) [26] and the l_o minimization in wavelet frame based model (l_o -WF) [43]. In Section 3.2, we perform the comparison on the simulation of image deblurring with our model, the l_o -WF model and the EDWF[44] model. For measuring the image quality quantitatively, we use the index peak signal to noise ratio (PSNR) defined by

$$PSNR := 10\log_{10}\left(\frac{255 * 255 * N}{\|ref - \tilde{u}\|_2^2}\right)$$

where ref and \tilde{u} are the true image and recovered image, respectively.

3.1 Image denoising

In this subsection, we compare the performances of our model with the SB, DTCWT, LHMM and l_o -WF on image denoising. Six images (all of size 256*256) shown in Figure 2 are tested. The noisy images are generated by the MATLAB command ‘imnoise’ with ‘type=Guassian’, $m = 0$ and variance $v = 0.01$.

In the implementation of image denoising, the parameters of our model are set as: $\lambda_0 = 12$, $\lambda_1 = 4.5$, $\gamma_0 = 2$, $\gamma_1 = 1.5$, $tol = 5e - 4$. For the SB algorithm, the parameters are set as: $\lambda = 19$, $gamma = 1$, $tol = 5e - 4$. For the DTCWT, the decomposition level $L = 4$, threshold $T = 20$. For the l_o -WF, the piecewise linear B-spline wavelet frame is also used and the decomposition level $L = 1$, $\lambda = 350$, $\mu = 1$, $\gamma = 0.2$, $tol = 5e - 4$.

In Figure 3, we show the feature (coefficient) images of a noisy image and its denoised version by our method. From Figure 3, we can see that the noises in every feature images are all removed.

In Figure 4 - Figure 6, we show the visual comparisons of the results from the four compared methods. From the results of SB, we can see that the recovered images have a lot of artifacts in the homogeneous regions. The reason is that the regularization parameter λ is chosen optimal for PSNR value. In order to preserve the sharp edges in images, a relatively small λ should be chosen. However, it leads to lack of smoothness in homogeneous regions. This visual effect is especially clear in the ‘cameraman’ image (see the sky and grass). From the results of DTCWT and LCHMM, we can observe that the restored images introduce too much artifacts. one of the reasons is that they both use the decimated wavelet transform. From the last two results, we can see that the denoised images by the l_o -WF and ours have similar visual effects, but our



Figure 2: The test images.

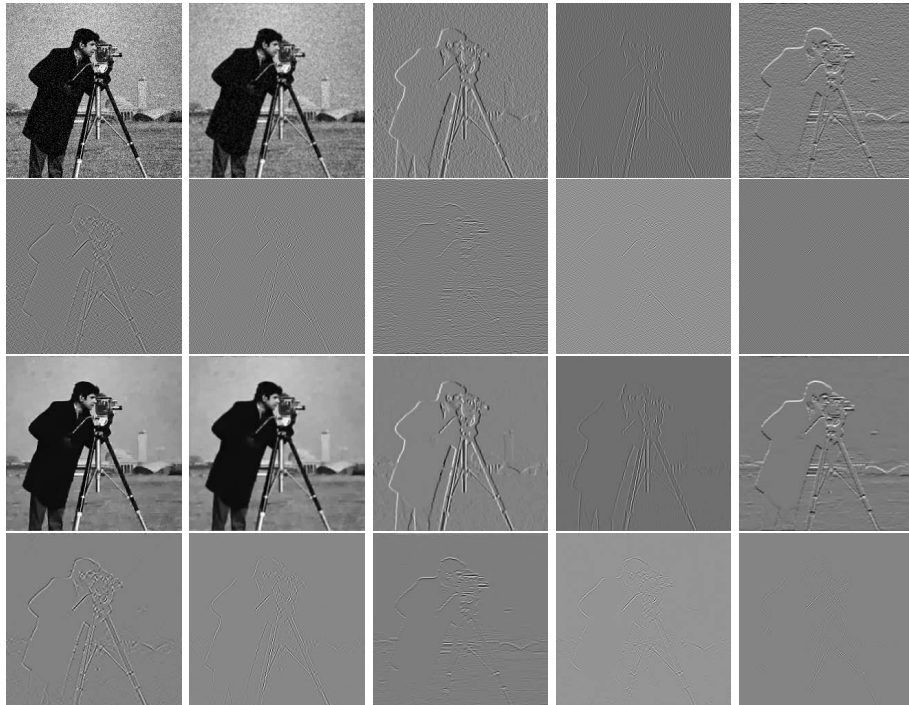


Figure 3: The feature images of the noisy and denoised.

method has a slightly higher PSNR and less runtime averagely which can be seen in Table 1.

Table 1 lists the PSNR and total run-time of the compared five methods for image denoising. Since the LCHMM is coded by C++ and the others by matlab, we don't list the runtime of LCHMM. From Table 1, we can see that our model outperforms the other image restoration methods in terms of PSNR, averagely. In addition, from Table 1, we can see that the DTCWT is the fastest (It spends less than 1 second for the six test images). However, the quality of the DTCWT is the worst. The PSNR of our model is about 1.4db higher than the DTCWT averagely.

To show the convergence of the modified split Bregman algorithm, we plot the relative error $\frac{\|u^{n+1} - u^n\|}{\|u^n\|}$ versus the iterations of the six test images in Figure 7. From Figure 7, we can observe the relative error is monotonically decreasing with the iterations, which numerically proves that the algorithm is convergent.

Table 1: PSNR of the compared four methods for image denoising

Image	original	SB	DTCWT	LCHMM	l_o -WF	our
1	20.45	27.05	26.21	27.14	27.63	27.81
2	20.04	30.20	28.45	29.78	31.17	30.99
3	20.07	25.64	25.28	26.00	25.88	26.36
4	20.15	26.16	25.78	26.47	26.40	26.69
5	20.06	27.64	27.09	27.98	27.98	28.18
6	20.17	27.89	27.17	28.08	28.20	28.33
average	20.17	27.43	26.66	27.57	27.88	28.06
Total Time(s)	-	3.09	0.49	-	12.40	4.02

3.2 Image deblurring

In this subsection, we apply the proposed model to image deblurring and compare the results with those of the l_o -WF and EDWF. We also test the same six images for image deblurring. The blurred images are generated by convolution with the blur kernel A and added by a Gaussian noise η , where A and η are generated by the MATLAB command ' $A = fspecial('motion', 9, 0)$ ' and ' $\eta = 5 * randn(size(u))$ ', respectively.

In the implementation of image deblurring, the parameters of our model are set as: $\lambda_0 = 0.4$, $\lambda_1 = 0.1$, $\gamma_0 = 0.004$, $\gamma_1 = 0.002$, $tol = 5e - 4$. For the l_o -WF, the piecewise linear B-spline wavelet frame is also used and the decomposition level $L = 1$, $\lambda = 30$, $\mu = 0.01$, $\gamma = 0.003$, $tol = 5e - 4$. For the EDWF, $\lambda = 1$, $\gamma = 1.5$, $\rho = 0.2$, $v = 0.15$, $\mu_1 = 1$, $\mu_2 = 1$.

In Figure 8, the visual results of the three models are presented and Table 2, summarizes the PSNR and total run-time of the three methods. From Table 2, we can see that the PSNR of our model is averagely the largest among the three methods. We can also observe from Table 2 that the run-time of our model is much less than the other two methods.



Figure 4: Comparison for image denoising. From left to right and up to down are: noisy images and denoised by SB, DTCWT, LCHMM, l_o -WF and ours, respectively.

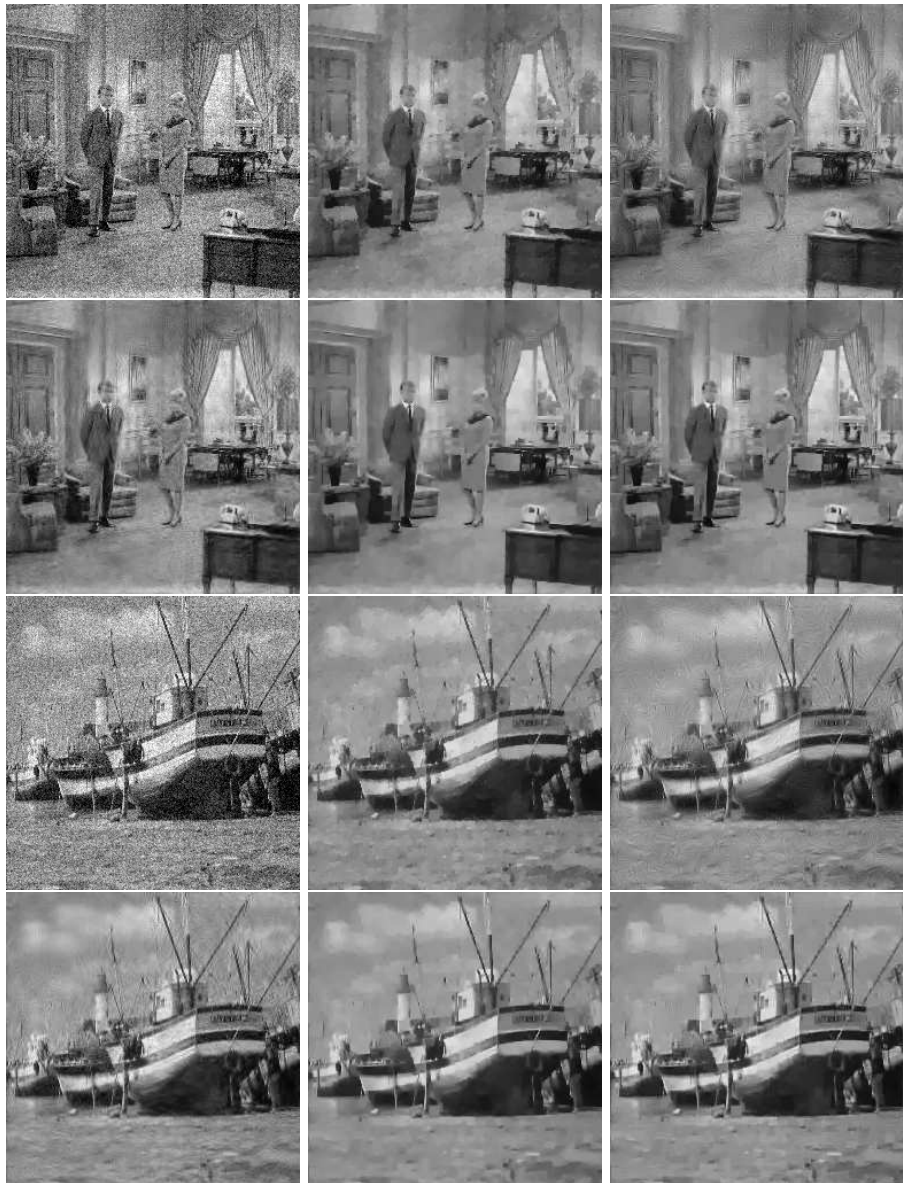


Figure 5: Comparison for image denoising. From left to right and up to down are: noisy images and denoised by SB, DTCWT, LCHMM, l_o -WF and ours, respectively.



Figure 6: Comparison for image denoising. From left to right and up to down are: noisy images and denoised by SB, DTCWT, LCHMM, l_o -WF and ours, respectively.

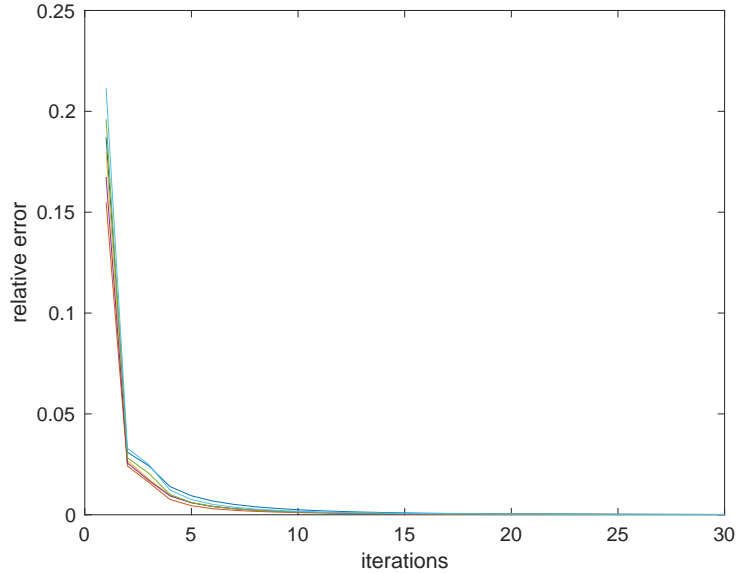


Figure 7: Relative error $\frac{\|u^{n+1} - u^n\|}{\|u^n\|}$ versus iterations of six test images.

Table 2: PSNR of the compared four methods for image deblurring

Image	original	l_o -WF	EDWF	our
1	21.43	26.25	26.16	26.85
2	26.50	32.55	31.77	32.61
3	22.75	25.60	25.44	25.98
4	22.57	25.39	25.31	25.82
5	24.28	28.07	27.70	28.17
6	22.63	27.73	27.56	28.02
average	23.36	27.60	27.32	27.91
Total Time(s)	-	26.67	141.34	7.76



Figure 8: Comparison for image deblurring. From left to right are: blurry images and deblurred by l_o -WF, EDWF and ours, respectively.

4 Conclusions

In this paper, we proposed a wavelet frame coefficient total variational model for image restoration and proved the existence of the solution of the model. A slightly modified split Bregman algorithm was used to solve the model. At last, we presented some experimental results to show its competitive advantage to the related methods both in quality and efficiency.

References

- [1] R. Choksi, Y. Van Gennip, and A. Oberman. Anisotropic total variation regularized l^1 -approximation and denoising/deblurring of 2D bar codes. *Inverse Problems & Imaging*, 5(3):591–617, 2017.
- [2] A. Marquina. Nonlinear inverse scale space methods for total variation blind deconvolution. *SIAM Journal on Imaging Sciences*, 2(1):64–83, 2009.
- [3] T. F. Chan and C. K. Wong. Total variation blind deconvolution. *IEEE Transactions on Image Processing*, 7(3):370–375, 1998.
- [4] Y. W. Wen, R. H. Chan, and A. M. Yip. A primal-dual method for total-variation-based wavelet domain inpainting. *IEEE Transactions on Image Processing*, 21(1):106–114, 2012.
- [5] M. Ng, F. Wang, and X. M. Yuan. Fast minimization methods for solving constrained total-variation superresolution image reconstruction. *Multidimensional Systems and Signal Processing*, 22(1):259–286, 2011.
- [6] K. Bredies and M. Holler. A total variation-based JPEG decompression model. *SIAM Journal on Imaging Sciences*, 5(1):366–393, 2012.
- [7] W. Wang and C. He. A variational model with barrier functionals for Retinex. *SIAM Journal on Imaging Sciences*, 8(3):1955–1980, 2015.
- [8] G. Gilboa and S. Osher. Nonlocal operators with applications to image processing. *SIAM Journal on Multiscale Modeling & Simulation*, 7(3):1005–1028, 2008.
- [9] S. M. Chao and D. M. Tsai. An improved anisotropic diffusion model for detail- and edge-preserving smoothing. *Pattern Recognition Letters*, 31(13):2012–2023, 2010.
- [10] C. Louchet and L. Moisan. Total variation as a local filter. *SIAM Journal on Imaging Sciences*, 4(2):651–694, 2014.
- [11] C. Sutour, C. A. Deledalle, and J. F. Aujol. Adaptive regularization of the nl-means: application to image and video denoising. *IEEE Transactions on Image Processing*, 23(8):3506–3521, 2014.

- [12] A. Chambolle. An algorithm for total variation minimization and applications. *Journal of Mathematical Imaging and Vision*, 20:89–97, 2004.
- [13] M. Zhu and T. F. Chan. An efficient primal-dual hybrid gradient algorithm for total variation image restoration. *UCLA Cam. Report*, 2008.
- [14] A. Beck and M. Teboulle. Fast gradient-based algorithms for constrained total variation image denoising and deblurring problems. *IEEE Transactions on Image Processing*, 18(11):2419, 2009.
- [15] E. Esser, X. Zhang, and T. F. Chan. A general framework for a class of first order primal-dual algorithms for convex optimization in imaging science. *SIAM Journal on Imaging Sciences*, 3(4):1015–1046, 2010.
- [16] T. Goldstein and S. Osher. The split bregman method for L1-Regularized problems. *SIAM Journal on Imaging Sciences*, 2(2):323–343, 2009.
- [17] A. Chambolle and T. Pock. A first-order primal-dual algorithm for convex problems with applications to imaging. *Journal of Mathematical Imaging and Vision*, 40(1):120–145, 2011.
- [18] W. Wang and C. He. A fast and effective algorithm for a poisson denoising model with total variation. *IEEE Signal Processing Letters*, 24(3):269–273, 2017.
- [19] J. F. Cai, S. Osher, and Z. Shen. Linearized bregman iterations for frame-based image deblurring. *SIAM Journal on Imaging Sciences*, 2(1):226–252, 2009.
- [20] C. Chaux, P. L. Combettes, J. C. Pesquet, and V. R. Wajs. A variational formulation for frame-based inverse problems. *Inverse Problems*, 23(4):1495, 2011.
- [21] M. J. Fadili, J. L. Starck, and F. Murtagh. Inpainting and zooming using sparse representations. *Computer Journal*, 52(1):64–79, 2009.
- [22] M. A. Figueiredo and R. D. Nowak. An EM algorithm for wavelet-based image restoration. *IEEE Transactions on Image Processing*, 12(8):906–16, 2003.
- [23] J. F. Cai, S. Osher, and Z. Shen. Split bregman methods and frame based image restoration. *SIAM Journal on Multiscale Modeling & Simulation*, 8(2):337–369, 2009.
- [24] M. Elad, J. L. Starck, P. Querre, and D. L. Donoho. Simultaneous cartoon and texture image inpainting using morphological component analysis (MCA). *Applied & Computational Harmonic Analysis*, 19(3):340–358, 2005.
- [25] J. L. Starck, M. Elad, and D. L. Donoho. Image decomposition via the combination of sparse representations and a variational approach. *IEEE Transactions on Image Processing*, 14(10):1570–82, 2005.

- [26] G. Fan and X.-G. Xia. Image denoising using a local contextual hidden markov model in the wavelet domain. *IEEE Signal Processing Letters*, 8(5):125–128, 2001.
- [27] J. F. Cai, R. Chan, L. Shen, and Z. Shen. Restoration of chopped and nodded images by framelets. *SIAM Journal on Scientific Computing*, 30(3):1205–1227, 2007.
- [28] J. F. Cai, R. H. Chan, and Z. Shen. A framelet-based image inpainting algorithm. *Applied & Computational Harmonic Analysis*, 24(2):131–149, 2008.
- [29] R. H. Chan, S. D. Riemenschneider, L. Shen, and Z. Shen. Tight frame: an efficient way for high-resolution image reconstruction. *Applied & Computational Harmonic Analysis*, 17(1):91–115, 2004.
- [30] A. Ron and Z. Shen. Affine systems in $l_2(r^d)$: The analysis of the analysis operator*. *Journal of Functional Analysis*, 148(2):408–447, 1997.
- [31] F. C. Tony and H.-M. Zhou. Total variation wavelet thresholding. *Journal of Scientific Computing*, 32(2):315–341, 2007.
- [32] K. Edoh and J. P. Roop. A fast wavelet multilevel approach to total variation image denoising. *International Journal of Signal Processing, Image Processing and Pattern Recognition*, 3(2), 2009.
- [33] H. Li, Z. Zhao, and X. Yu. A novel image denoising algorithm in wavelet domain using total variation and grey theory. *Engineering Computations*, 27(7):863–877, 2010.
- [34] Y. W. Wen, R. H. Chan, and A. M. Yip. A primal-dual method for total-variation-based wavelet domain inpainting. *IEEE Transactions on Image Processing*, 21(1):106–114, 2012.
- [35] N. Bhoi and D. S. Meher. Total variation based wavelet domain filter for image denoising. *First International Conference on Emerging Trends in Engineering and Technology*, pages 20–25, 2008.
- [36] G. R. Easley, D. Labate, and F. Colonna. Shearlet based total variation for denoising. *IEEE Transactions on Image Processing*, 18(18):260–268, 2009.
- [37] C. Vonesch and M. Unser. A fast multilevel algorithm for wavelet-regularized image restoration. *IEEE Transactions on Image Processing*, 18(3):509–523, 2009.
- [38] Y. Ding and I. W. Selesnick. Artifact-free wavelet denoising: Non-convex sparse regularization, convex optimization. *IEEE Signal Processing Letters*, 22(9):1364–1368, 2015.

- [39] S. Amat, J. Ruiz, and J.C. Trillo. Fast multiresolution algorithms and their related variational problems for image denoising. *Journal of Scientific Computing*, 43(1):1–23, 2010.
- [40] J. Xu and S. Osher. Iterative regularization and nonlinear inverse scale space applied to wavelet-based denoising. *IEEE Transactions on Image Processing*, 16(2):534–544, 2007.
- [41] L. Vese. A study in the BV space of a denoising-deblurring variational problem. *Applied Mathematics and Optimization*, 44(2):131–161, 2001.
- [42] I. W. Selesnick, R. G. Baraniuk, and N. C. Kingsbury. The dual-tree complex wavelet transform. *IEEE Signal Processing Magazine*, 22(6):123–151, 2005.
- [43] B. Dong and Y. Zhang. An efficient algorithm for l_0 minimization in wavelet frame based image restoration. *Journal of Scientific Computing*, 54(2-3):350–368, 2013.
- [44] J. K. Choi, B. Dong, and X. Zhang. An edge driven wavelet frame model for image restoration. *arXiv:1701.07158*, 2017.